A New Approach to HF Channel Modeling and Simulation

Part I: Deterministic Model

L.E. Vogler
J.A. Hoffmeyer

CONTENTS

LIST OF FIGURES

A NEW APPROACH TO HF CHANNEL MODELING AND SIMULATION
PART I: DETERMINISTIC MODEL

L. E. Vogler and J. A. Hoffmeyer[*]

This report describes a new and unique approach for modeling either narrowband or wideband high frequency (HF) channels. Although narrowband models of the HF channel have existed for many years, they are applicable to only a limited set of actual propagation conditions. The need for an HF channel model that is valid for both narrow and wide bandwidths over a more extensive range of propagation conditions provided the motivation for the research documented in this report.

The report describes the development of a channel transfer function for the HF channel that accurately models a wide variety of propagation conditions and can be used for the evaluation of wideband HF systems. The first part of this modeling effort has been to develop a model that represents the median channel conditions. Good agreement has been found between the model and wideband propagation measurements taken during relatively stable conditions. The report provides comparisons between ionograms generated by the model and measured wideband ionograms that have been reported in the literature. Encouraging results have also been found in comparing model outputs with measured time-history plots.

Key words: channel transfer function; HF channel models; HF propagation; over-the-horizon radar (OTHR); spread spectrum; wideband communications; wideband HF

1. INTRODUCTION

For many years, the high frequency (HF) channel model and channel simulation techniques developed by C. Watterson have been utilized for the laboratory performance evaluation of narrowband high frequency communication systems. This narrowband model, its implementation in both hardware and software simulators, and the use of these simulators in HF system performance evaluation have been widely reported in the literature (Watterson, 1981 and 1982; Watterson and Coon, 1969; Watterson et al., 1969 and 1970; CCIR, 1974; Ehrman et al., 1982; Mooney, 1985; Girault et al., 1988; McRae and Perkins, 1988; LeRoux et al., 1987). Despite the model's apparent usefulness, it is

---

[*]The authors are with the Institute for Telecommunication Sciences, National Telecommunications and Information Administration, U.S. Department of Commerce, Boulder, CO 80303-3328.

valid only for system bandwidths of 12 kHz or less under limited conditions. Interest in the application of spread spectrum technology to HF systems provided the initial motivation for the investigation of channel models that accurately represent a wideband (greater than 12-kHz) HF channel (Hoffmeyer and Nesenbergs, 1987).

The requirement for the use of wide bandwidths in HF systems needs further discussion. The employment of wideband signals has advantages for both communications and over-the-horizon radar (OTHR) signals if

(1) the HF media can support the propagation of such signals,

(2) the transmission of such signals do not interfere with other users in the band, and

(3) the effects of external noise and interference in the wideband channel can be mitigated through the use of appropriate signal processing.

For communication systems, the advantages of spread-spectrum technology are well known (Dixon, 1984). These advantages include low-probability-of-intercept (LPI) communications, interference rejection, simultaneous operation of several transmitters in the same frequency band, and resolution of multipath sky-wave returns. For HF radar systems, the use of wideband spread-spectrum signals results in improved range resolution. Thus, both applications require the use of the widest possible bandwidth for a given path, time of day, season, sunspot number, etc.

There are many uncertainties regarding the attainable performance of either wideband HF communications systems or extended bandwidth OTHR systems. A capability to evaluate the potential performance of such systems without the cost of building the hardware and running extensive field tests is needed. Such performance evaluation can best be attained through the use of channel simulation. The advantages of channel simulators for the testing of communication systems are well known (Hoffmeyer and Vogler, 1987; Watterson, 1981). The advantages include accuracy, repeatability, stationarity, availability, parameter variation, and cost. Thus, a wideband HF channel model that has been validated by wideband channel measurements is needed.

Research programs in wideband HF have followed four parallel but strongly interconnected paths:

- development and field testing of experimental wideband communication systems
- channel noise and interference measurement and modeling programs
- wideband channel propagation measurement programs
- channel transfer function modeling programs

Perry et al. (1987) describe experimental wideband HF communication systems. Vogler et al. (1988) and Perry and Abraham (1988) describe approaches to noise/interference modeling programs. Our primary interest in this report is in channel transfer function modeling.

Numerous wideband HF channel propagation measurement programs are being conducted in the United States, Norway, and the United Kingdom (Wagner et al., 1983; Wagner and Goldstein, 1985; Wagner et al., 1987a and 1987b; Wagner, 1987; Haines and Weijers, 1985; Baker et al., 1986; Salous and Shearman, 1986; Skaug, 1982 and 1984). The apparent objectives of these programs are to provide data useful for the understanding of the HF channel and for the eventual development of spread-spectrum HF systems. These data are also critically needed for the development of a validated wideband HF channel model. The channel probe developed at the Naval Research Laboratory (Wagner et al., 1983) has the highest resolution of any of the measurement systems described in the above references. The Institute for Telecommunication Sciences has been provided with NRL wideband HF channel probe data and the use of these data in the development of a wideband channel model will be described in Section 4.

The emphasis in this report is on the channel transfer function modeling, which is strongly dependent on empirical propagation measurement data. This can be seen in Figure 1 which depicts the interrelationship between the required measurements, the wideband high frequency (WBHF) models, and both hardware and software implementations of those models. The two parts of the WBHF modeling process are the propagation model or channel transfer function and the noise and interference models. Only the channel transfer function portion of the model will be discussed in this report. A description of the work that has been accomplished at ITS in the development of a wideband HF noise and interference model may be found in Vogler et al. (1988).

The channel transfer function and noise and interference models can be implemented in either software or hardware. Software implementations of the models are useful during the system design phase of, for example, a wideband HF

3
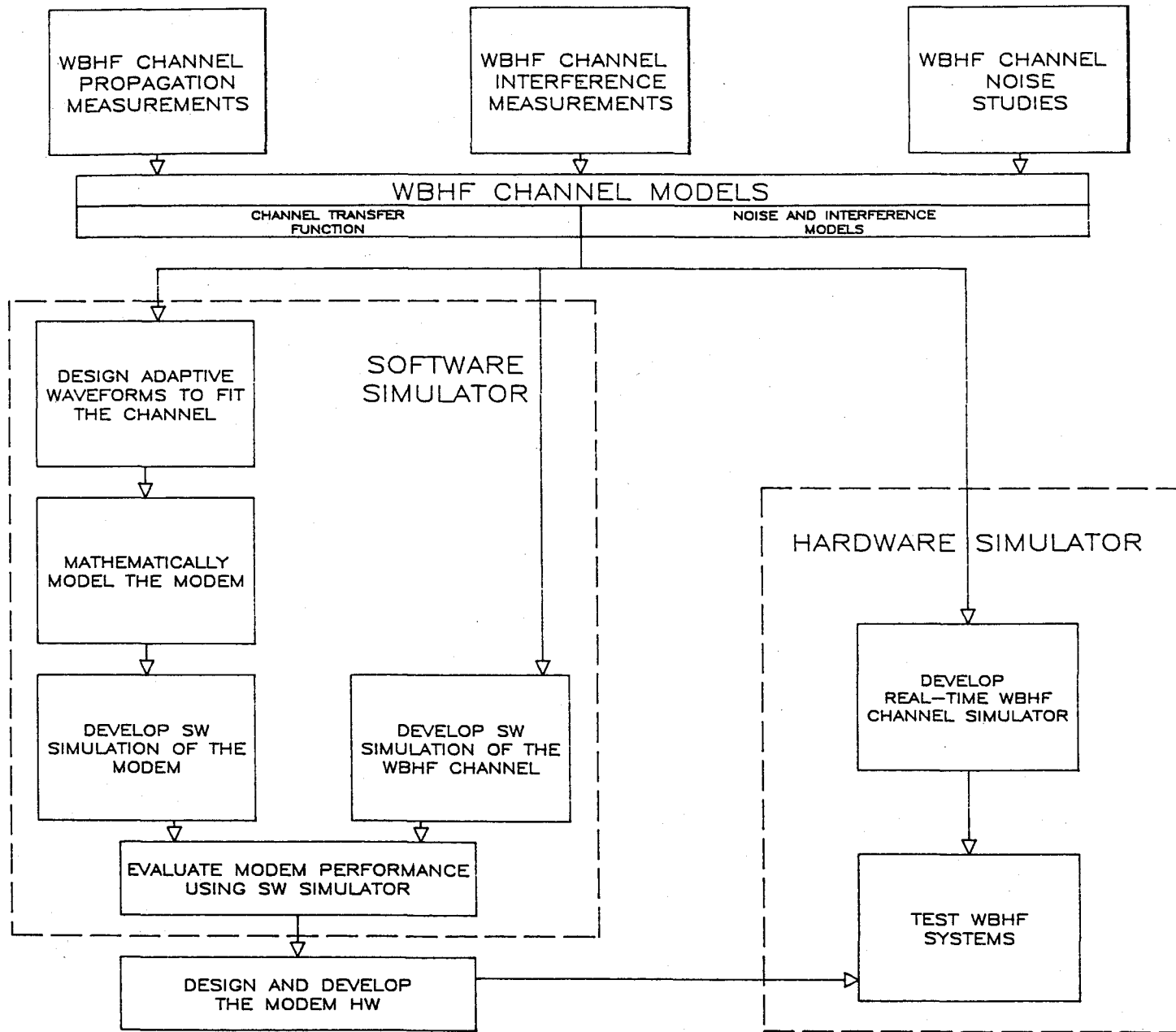
Figure 1.   Interrelationship of wideband HF channel measurements, modeling, and simulation programs.

TX   RX

HF freq dispersive medium
—pulses smeared
only the w. the resp to different freq

modem. If the HF system as well as the WBHF models are implemented in a software simulator, the theoretical performance of various modem designs can be evaluated. Hardware implementations of the models are useful in the performance testing of the complete HF system hardware. A logical sequence of events would be the use of a software simulator during the design phase of a wideband HF system and a hardware simulator to evaluate the performance after the chosen design has been implemented in hardware.

Watterson: smear w resp.
to 1) doppler -dϕ/dt
or 2) density of layer.

## 1.1 Application of Watterson Model

One possible approach to the development of a wideband channel model would be to attempt to extend the valid bandwidth of the Watterson model. The channel transfer function for this model is given by

Amp — dependent only on time - diurnal, seasonal,
phase — gaussian freq dep

$$H(f,t) = \Sigma_n c_n(t) \exp[-i2\pi\tau_n f] \qquad (1)$$

where $c_n(t)$ are time varying tap gain functions, and τ_n is the time delay for the n_{th} propagation path and is not a function of frequency.

single value
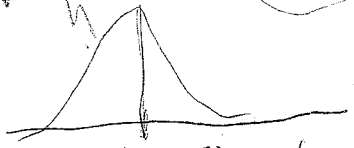
$v \sim$ doppler effect   doppler freq — derivitive of phase w resp to time

Although this approach is appealing and could possibly be achieved, some difficulties are expected. One problem is finding a representation for the tap gain multipliers, $c_n(t)$, of (1). As noted earlier, the Watterson model was validated for only a limited set of propagation conditions and, even for a narrowband HF channel, measured propagation data could be fit to a Gaussian distribution only with significant restrictions. At times an adequate fit could be obtained only for a 2.5-kHz bandwidth (see Table 1). Therefore, the likelihood of finding a distribution that would fit the measured data for much wider bandwidths (12 - 1000 kHz) is low.

As has been noted by other researchers, there are restrictions on the general applicability of the Watterson model (LeRoux et al., 1987). The model is representative of the HF channel only when the channel may be considered to be stationary and stable. In the validation of the model, Watterson selected data that "seemed most nearly stationary in terms of fading rates, modal time delays, and average power in the modes" (Watterson et al., 1969). In summary, the model is limited to

- channel bandwidths of 12 kHz or less

N: modes — hops, ordinary/extraordinary 2 reflections
for 1 hop path, 2 modes

Table 1. Validation of Watterson Model

Sample	Period	Tx. Frequency (MHZ)	Valid Bandwidth
1	13 minutes (daytime)	9.259 MHZ	12.0 kHZ
2	10 minutes (daytime)	9.259 MHZ	8.0 kHz
3	13 minutes (evening)	5.864 MHZ	2.5 khz

One path: Long Branch, IL, to Boulder, CO (1294 km)

One season: November, 1967

- channels having time and frequency stationarity
- channels having negligible delay dispersion (e.g., no spread-F)
- channels having only a low-ray path

Approximately 20 years have passed since the Watterson model was originally developed. Unfortunately, with the passage of time, it appears that the restrictions on the use of the model are sometimes forgotten. The restrictions, even for narrowband applications, have provided further motivation for the development of an entirely new HF channel model. The new model should have general applicability to a wide variety of propagation conditions and channel bandwidths.

The limitations of the Watterson model, particularly in regard to its validated bandwidth, and the recent interest in wide bandwidth HF have provided motivation for researchers in a number of organizations to investigate either extensions to the model or entirely new models (Serrat-Fernandez et al., 1985; Malaga, 1985; Barratt and Walton, 1987; and Hoffmeyer and Nesenbergs, 1987). Serrat-Fernandez et al. (1985), for example, propose a slight modification of the Watterson model in which the Gaussian shape of the Doppler spectrum is replaced by a Butterworth shape. The assumption, valid for narrowband models, that the group delay is not a function of frequency is also an area of current interest. Clearly, this assumption does not hold for wideband HF. The methodology for modeling this and other parameters for the wideband case is the target of research and the subject of the remainder of this paper.

The modeling approach we have taken is outlined below and discussed in detail in Sections 2 through 4. Our model, the Ionospheric Parameters Model (IPM), is a model that relates the quantities of the transfer function to actual physical parameters of the ionosphere. As will be demonstrated in Section 4, the model is capable of representing the channel under a variety of propagation conditions, path geometries, and bandwidths.

In any wideband HF simulation model, the relationship between delay time and frequency is of major importance. The frequency components of a pulse reflected from the ionosphere arrive at the receiver with different delay times, thus causing a distortion of the original pulse shape. For narrow bandwidths (e.g., 3 kHz), the effect of the delays (caused by frequency dispersion) on the shape is generally negligible. However, there can be considerable effect on signals having bandwidths of the order of 100 kHz or more (Wagner and Goldstein, 1985). If a true impulse could be transmitted, the impulse response would have a very broad shape because of the delays encountered by all the frequencies in the "infinite" bandwidth. An indication of the broadening of the impulse response can be obtained from the examination of a typical ionogram (see Section 4).

1.2 Ionospheric Parameters Model

A disadvantage in the extension of the Watterson model approach is the difficulty of getting quantitative estimates for the delay time vs. frequency relationship. A suggested procedure is to measure the slope of an ionogram trace over the bandwidth of interest. This works as long as there are stable conditions and the noise threshold is fairly constant.

The Ionospheric Parameters Model approach provides an analytic expression for the delay-frequency relation that serves as a long-term median or deterministic base around which statistical variations can be added. The analysis is based on a well-known electron density model and can be related to the physical parameters for each of several ionospheric layers. Thus, it is a variable base applicable to many different seasons and locations. The model can utilize the extensive information fund already available concerning the deterministic and statistical characterizations of ionospheric parameters.

The use of an analytic expression for the phase was suggested many years ago in a paper by Wetzel (1967) in which he assumed a parabolic layer model for

the electron density profile. The parabolic model provides a fairly realistic description of a stable ionospheric layer; however, the equation relating delay time and frequency requires iterative procedures to evaluate. On the other hand, the corresponding equation derived for the IPM is an explicit expression for the frequency in terms of the delay time. The following section describes the mathematical derivation of the channel transfer function for the IPM.

2. TRANSFER FUNCTION

2.1 Ionospheric Parameters Model

A symbolic representation of the transfer function $H(\omega,t)$ of an ionospheric reflection channel can be expressed as

$$H(\omega,t) = \sum_n H_n(\omega,t), \tag{2}$$

where $H_n(\omega,t)$ denotes the transfer function of a particular path or mode in the channel, and $\omega = 2\pi f$ is the (angular) frequency. Variations of the ionosphere's physical constituents over time are represented by the symbol t. In most of the following discussion, the derivations refer to a single path or mode, and the subscript n is suppressed.

In the present case, the transfer function will be formulated as the summation of reflection coefficients $R(\omega) = H_n(\omega)$, t constant, associated with the different layers of the ionosphere. In general the coefficients depend on electron density, collision frequency, Earth's magnetic field, and the geometry of the propagation path. If all of these quantities were constant over time for a given channel, then the transfer function and, thus, signal response could be evaluated deterministically because of the stable conditions. However, a model applicable to actual channels requires a statistical description due to time variations of the physical processes. The utility of the model will be enhanced if the deterministic base, around which the statistical variations are applied, can provide "long term" or median values appropriate to a wide variety of propagation conditions.

A model that has been used to approximate the electron density profile of a single ionospheric layer is the $sech^2$ model (Budden, 1961, p. 156):

$$f_N^2 = f_p^2 \, sech^2\{(z_m-z)/2\sigma\}, \tag{3}$$

8

where f_N^2 is proportional to the electron density and z denotes height above a reference plane on the propagation path. The maximum electron density occurs at the height z_m and, thus, f_p denotes the penetration frequency. The general shape of the profile is displayed in Figure 2, which also shows how the thickness of the layer can be altered by using different values of the scale height parameter σ.

By varying the layer height, thickness, and maximum electron density parameters of the $sech^2$ model, one can approximate a wide variety of single layer configurations. An exact expression for the ionospheric reflection coefficient can be derived from Maxwell's equations for the case of no magnetic field and negligible collision frequency. Under certain conditions, an exact expression is possible even with the latter two quantities included (Vogler, 1984); however, the resultant function is difficult to handle in a simulation model and will not be considered in the present study.

The exact coefficient is a ratio of complex gamma functions $\Gamma(\cdot)$ (Abramowitz and Stegun, 1964, p. 255) and, for vertical incidence, is given by

$$R(\omega) = -\frac{\Gamma(1-i\alpha\omega)\Gamma(1/2-\chi+i\alpha\omega)\Gamma(1/2+\chi+i\alpha\omega)}{\Gamma(1+i\alpha\omega)\Gamma(1/2-\chi)\Gamma(1/2+\chi)}e^{-i\omega t_o}, \tag{4}$$

where $\alpha = 2\sigma/c$, $\chi = (i/2)\{(2\alpha\omega_p)^2-1\}^{1/2}$, $t_o = (2/c)z_m$, and c is the speed of light in free space.

Equation (4) is still too complicated to use as a deterministic base for the transfer function in our simulation model even with the conditions that have been imposed. However, it can be shown that the absolute value of (4) varies only slowly over most of the frequency range of interest and, furthermore, asymptotic formulas of the gamma function (Abramowitz and Stegun, 1964, p. 257) can be used to simplify the phase portion. Thus, we may write

$$R(\omega) = |R(\omega)|e^{i \text{ arg } R} \approx |R(\omega)|e^{-i\phi(\omega)}, \tag{5}$$

$$\phi(\omega) = \omega t_o - \alpha[\omega \ln\{(\omega_p/\omega)^2-1\}+\omega_p \ln\{(\omega_p+\omega)/(\omega_p-\omega)\}], \tag{6}$$
$$\text{(vertical incidence)}$$

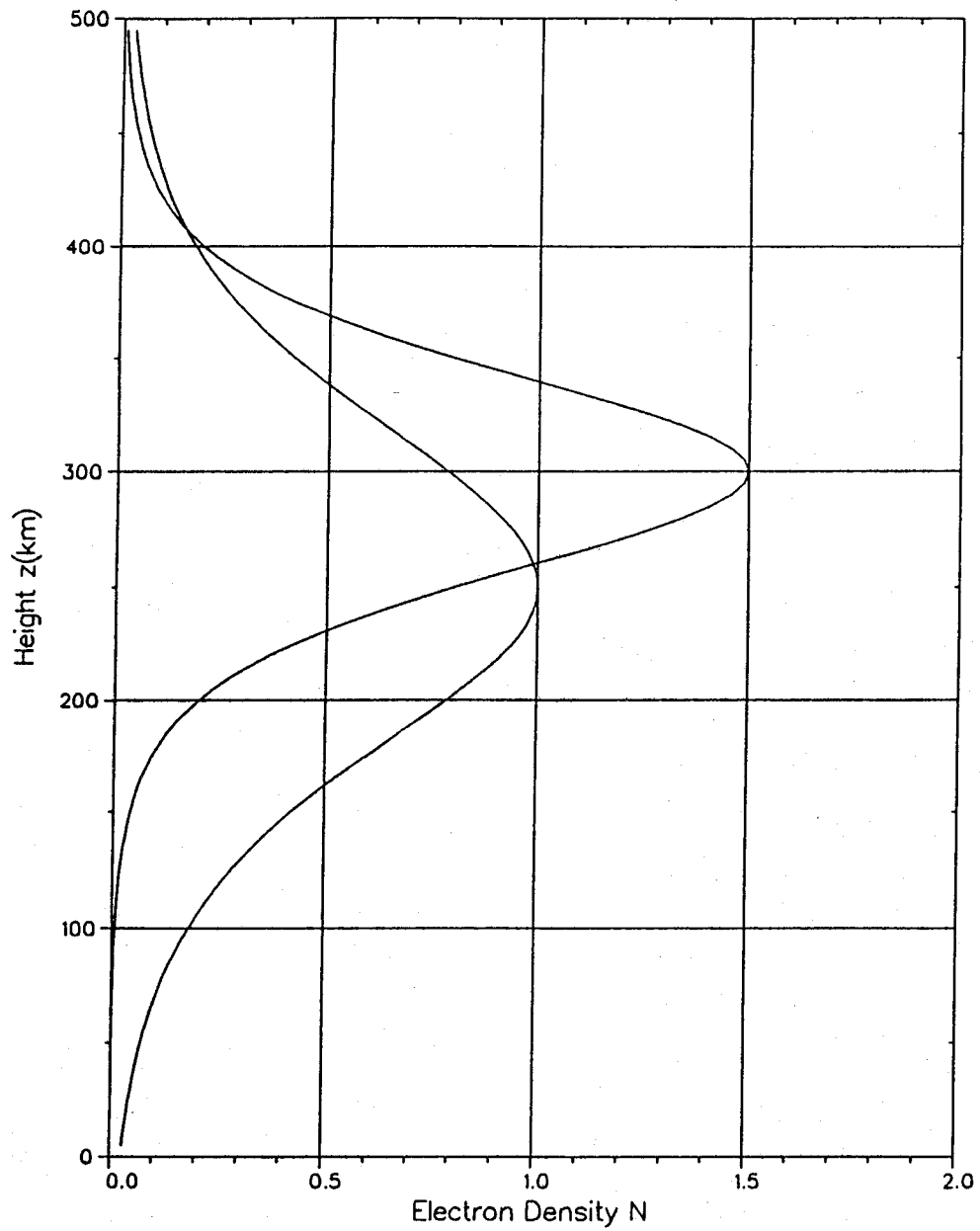$$\phi'(\omega) = d\phi/d\omega = t_o - \alpha \ln\{(\omega_p/\omega)^2-1\}. \tag{7}$$

9

Figure 2. Electron density profile for a sech^2 model. The density N is in cm^{-3}, and the abscissa should be multiplied by 10^6. The values of σ(km) for the narrow and wide curves are 30 and 50, respectively.

An alternative way of arriving at (6) and (7) is described in the Appendix.

The first derivative of ϕ is associated with the reflection time of frequency components of the transmitted signal, and it is usual to define an equivalent height of reflection, $\bar{h}(\omega)$, to represent the (apparent) height at which the component is reflected back to the receiver:

$$\bar{h}(\omega) = (c/2)\phi'(\omega) = h_o - \sigma\ln\{(\omega_p/\omega)^2 - 1\}, \text{ (vertical incidence)} \tag{8}$$

where $h_o = ct_o/2$. (The usual notation for equivalent height is h', but we here have reserved the prime to denote differentiation).

The above discussion has assumed vertical incidence with the signal being transmitted and received at the same site. The problem of timing the frequency components of a pulse over an oblique path of distance D between terminals is resolved by applying the theorems of Breit and Tuve and of Martyn (Kelso, 1964, pp. 220-226):

$$\bar{P}(\omega) = D/\sin\theta_I, \text{ (Breit and Tuve)} \tag{9a}$$

$$\bar{h}(\omega) = \bar{h}(\omega_v) = \bar{h}, \text{ (Martyn)} \tag{9b}$$

$$\omega = \omega_v \sec\theta_I = \omega_v\{1+(D/2\bar{h})^2\}^{1/2}, \tag{9c}$$

where θ_I is the incidence angle of the ray (for vertical incidence, $\theta_I = 0$), and $\bar{P}(\omega)$ is the equivalent path for the ω component, i.e., the distance from the transmitter to the reflection height $\bar{h}$ and back to the receiver. The notation ω_v refers to the frequency associated with vertical incidence.

From (8) the relationship between ω_v and $\bar{h}$ is seen to be

$$\omega_v = \omega_p[1+\exp\{(h_o-\bar{h})/\sigma\}]^{-1/2}, \tag{10}$$

and from (9c) it follows that

$$\omega = \omega_p\{1+(D/2\bar{h})^2\}^{1/2}[1+\exp\{(h_o-\bar{h})/\sigma\}]^{-1/2}. \tag{11}$$

Thus, if for notational convenience, we introduce the functions

11

$$\nu = \nu(\bar{h}) = 1+(D/2\bar{h})^2 , \quad \delta = \delta(\bar{h}) = 1+\exp\{(h_o - \bar{h})/\sigma\}, \tag{12}$$

then the travel time over the oblique path of that component of the signal with angular frequency ω is given by

$$\bar{P}(\omega)/c = (2/c)\bar{h} \sec\theta_I = (2\bar{h}/c)(\nu)^{1/2}, \tag{13}$$

and the relationship between ω and the effective height $\bar{h}$ is

$$\omega = \omega_p \{\nu/\delta\}^{1/2}. \tag{14}$$

As mentioned before, the reflected travel time is associated with the first derivative of the phase in the reflection coefficient (5):

$$\phi'(\omega) = d\phi/d\omega = \bar{P}(\omega)/c = (2\bar{h}/c)(\nu)^{1/2}, \tag{15}$$

and, in fact, (15) reduces correctly to (7) in the case of vertical incidence (D = 0). The phase function, $\phi(\omega)$, can now be expressed as

$$\phi(\omega) = \int \phi'(\omega)d\omega. \tag{16}$$

In the general case of oblique incidence, (16) must either be evaluated numerically or approximated by simpler functions, the latter alternative being used in the present computer implementation of the simulation model. Through the use of (12) and (14), $\bar{h}$ is put into suitable forms for the low ray and for the high ray:

$$\bar{h} = h_o - \sigma \ln\{(\omega_p/\omega)^2\nu - 1\}, \quad \text{(low ray)} \tag{17a}$$

$$\bar{h} = (D/2)\{(\omega/\omega_p)^2\delta - 1\}^{-1/2}. \quad \text{(high ray)} \tag{17b}$$

Approximations to ν and to δ, respectively, are then made and $\phi \approx \phi_{lo}$ or $\phi \approx \phi_{hi}$ is obtained from (15) and (16). For the present comparisons, first order approximations to ϕ were made by setting ν and δ constant in (17).

For instance, for the low ray with

$$\nu \approx \text{const} = \nu_o = 1+(D/2h_o)^2, \tag{18a}$$

$$\overline{h} \approx \overline{h}_o = h_o - \sigma \ln|(\omega_p/\omega)^2 \nu_o - 1|, \tag{18b}$$

(16) may be integrated to yield

$$\phi_{1o}(\omega) \approx \alpha\omega_p\nu_o[(\overline{h}_o/\sigma\rho_o) - \ln|(\rho_o+1)/(\rho_o-1)|], \tag{19}$$

where $\rho_o = (\omega_p/\omega)(\nu_o)^{1/2}$. This reduces to (6) for vertical incidence. Similarly, with

$$\delta \approx \delta_o (= \text{const}), \quad \nu \approx (\omega/\omega_p)^2 \delta_o, \tag{20a}$$

$$\overline{h} \approx (D/2)\{(\omega/\omega_p)^2\delta_o - 1\}^{-1/2}, \tag{20b}$$

ϕ for the high ray is found to be

$$\phi_{hi}(\omega) \approx (D/c)\{\omega^2 - \omega_p^2/\delta_o\}^{1/2}. \tag{21}$$

The above equations for ϕ can be used to compute a deterministic base for each term of the transfer function (2) by setting $H_n(\omega) = R_n(\omega)$ from (5). It is important to notice that the statistical variations with time of the physical parameters h_o, σ, and f_p provide the t dependence of the channel transfer function.

2.2 Other Models

The technique in which the transfer function phase is expanded in a Taylor's series around some convenient frequency ω_o was used many years ago in one of the earlier papers on HF propagation modeling (Wetzel, 1967). Because frequency dispersion was the primary interest, variation over time was not considered. However, the approach is still valid if the dependence on time is understood to arise from changes in the positions and magnitudes of the physical quantities describing the ionosphere.

13

Following Wetzel, and suppressing the t dependence for notational convenience, we have

$$\phi_n(\omega,t) = \phi_n(\omega_o) + \phi_n'(\omega_o)(\omega-\omega_o) + \hat{G}_n(\omega-\omega_o)$$

$$= \Theta_n(\omega,t) + \omega\phi_n'(\omega_o), \tag{22}$$

where $\hat{G}_n(\omega-\omega_o)$ includes all higher order terms in the Taylor expansion. The nth mode of the transfer function is then

$$H_n(\omega,t) = |H_n(\omega,t)| e^{-i\phi_n(\omega,t)}$$

$$= A_n(\omega,t) e^{-i\{\Theta_n(\omega,t)+2\pi f \tau_n(\omega_o)\}}, \tag{23}$$

where $\tau_n(\omega_o) = \phi_n'(\omega_o) = (d\phi_n/d\omega)|_{\omega_o}$ is the delay time and $A_n = |H_n|$. Specifying particular functions for A_n and Θ result in the various simulation models that have been proposed.

For instance, the nth node of the narrowband model of Watterson et al. (1970) can be written as

$$H_n(f,t) = G_n(t) e^{-i2\pi f \tau_n}, \tag{24a}$$

$$G_n(t) = G_{no}(t) e^{i2\pi\nu_{no}t} + G_{nx}(t) e^{i2\pi\nu_{nx}t}, \tag{24b}$$

where G_{no} and G_{nx} are Gaussian random processes with arbitrarily chosen amplitudes and Doppler frequency spreads, and O or X refers to the ordinary or extraordinary mode, respectively. The amplitudes, spreads, and Doppler frequency shifts $\nu_{no,x}$ are functions of the time correlation interval, but neither these nor the delay time τ_n depends on signal frequency. Thus, $G_n(t)$ corresponds to $A_n(t) \exp\{-i\Theta_n(t)\}$ in (23) with no ω (or f) dependence.

A wideband propagation model proposed by Malaga (1985) specifies the delay time τ_n as a function of frequency as in (23) and replaces Θ_n by

$$-\Theta_n(\omega,t) = \hat{\phi}_n(f_o,t) + 2\pi\nu_n(f_o,t)t, \tag{25a}$$

$$H_n(f,t) = A_n e^{i\{\hat{\phi}_n(f_o,t)+2\pi\nu_n(f_o,t)t\}} e^{-i2\pi f\tau_n(f_o)}, \tag{25b}$$

where $\hat{\phi}_n$ represents phase fluctuations with Gaussian statistics, and the Doppler shift ν_n is a function of frequency and the time rate of change of the phase path length. Note the correspondence between $A_n \exp\{i\hat{\phi}_n(f_o,t)\}$ in Malaga's model and $G_{no}(t)$ or $G_{nx}(t)$ in the narrowband representation of (24b); A_n, of course, is understood to be a function of both time and frequency in the wideband model.

3. RECEIVED SIGNAL

3.1 IPM Pulse Response

In order to test the adequacy of a model for the transfer function, it is desirable to compare the predicted pulse response with actual measurements. For a received signal $E_r(\tau)$ normalized by a constant amplitude E_o, the pulse response for the attenuation $A(\tau)$ may be written as

$$E_r(\tau)/E_o = A(\tau) = (1/2\pi)\int_{-\infty}^{+\infty} S_T(\omega)H(\omega)S_R(\omega)e^{i\omega\tau}d\omega, \tag{26}$$

where $S_T(\omega)$, $S_R(\omega)$ denote the source and receiver frequency responses and $H(\omega)$ is the channel transfer function. Most pulse sounders measure only the group delay of a propagating mode, resulting in the usual ionogram trace of time delay versus frequency. The recently developed NRL Channel Prober (Wagner and Goldstein, 1985) measures group delay, amplitude, and delay dispersion for wideband or narrowband pulses and for either vertical or oblique incidence. Thus, results from this instrument can be used to investigate the usefulness of a proposed model.

It is not possible, in general, to represent the integral of (26) in closed form, and some type of approximation is necessary. Numerical integration, using a Fast Fourier Transform, is usually adequate if one is restricted to lower frequency components, but this becomes unwieldy at higher frequencies. The most satisfactory solution, at least for a model based on a sech[2] electron density profile (Vogler, 1985), is the method of stationary phase. This approach takes advantage of the fact that the major contribution to the integral occurs near those frequencies where the first derivative of the

15

phase of the integral equals zero (Papoulis, 1962, pp. 139-141). When applied to (26), the result is

$$A(\tau) \approx \sum_{\omega_o} F(\omega_o) |2\pi\Phi''(\omega_o)|^{-1/2} e^{i\{\Phi(\omega_o) - \omega_o \Phi'(\omega_o) \pm \pi/4\}}, \tag{27}$$

$$\text{where } F(\omega) = |S_T(\omega)H(\omega)S_R(\omega)|, \tag{28a}$$

$$\Phi(\omega) = \arg S_T(\omega) + \arg H(\omega) + \arg S_R(\omega), \tag{28b}$$

$$\Phi'(\omega_o) + \tau = 0, \tag{28c}$$

and the primes denote differentiation with respect to ω. The summation is over all values of ω_o that satisfy (28c).

The stationary phase method yields a good approximation to the pulse response as long as $F(\omega)$ is not oscillatory near the roots $\omega = \omega_o$. For the comparison examples presented here, $|H(\omega)|$ is nearly constant over the whole frequency range of interest. The receiver frequency response is assumed to be ideal in the sense that its only effect is to place a constant valued "ceiling" and "floor" on the received signal amplitude. The source pulse is taken to be Gaussian shaped with an arbitrarily chosen pulse width and center frequency. Other source and receiver responses may be assumed, of course, but their numerical behavior must follow the above qualifications if (27) is to be used.

A display of the pulse response can be shown in a three-dimensional format equivalent to the NRL Channel Prober outputs in Wagner and Goldstein (1985). The amplitude is plotted versus time delay and center frequency of the source pulse resulting in a three-dimensional ionogram. The receiver threshold and AGC are simulated by the receiver "floor" and "ceiling" mentioned above, and the threshold level that is chosen can affect the width of the received dispersed pulse.

In the present comparisons, we set $\arg S_T(\omega)$ and $\arg S_R(\omega)$ to zero and assume $H(\omega) \approx \exp\{-i\phi(\omega)\}$. The expressions used in computing an impulse response then depend on the input parameters representing the layer height and thickness (h_o and σ), the penetration frequency f_p, and the path distance D. A key relationship that describes the trace of a delay time versus frequency (τ vs f) ionogram can be derived from (14), (15), and (28c):

16

$$\overline{h}_\tau = \{(c\tau/2)^2 - (D/2)^2\}^{1/2}, \tag{29}$$

$$\omega_\tau = \omega_p \{\nu_\tau/\delta_\tau\}^{1/2}, \tag{30}$$

$$\nu_\tau = \nu(\overline{h}_\tau), \quad \delta_\tau = \delta(\overline{h}_\tau), \tag{31}$$

with ν and δ given by (12). For a given value of τ, ω_τ can be found from (30). Alternatively, one could choose ω_τ and then compute the corresponding delay time τ, although in this case, a root-finding procedure is necessary to calculate the equivalent height $\overline{h}_\tau$. Note that the minimum τ must be greater than D/c, the time taken to transverse the straight line distance between terminals.

A maximum frequency ω_M occurs as $\overline{h}_\tau$ in (30) increases. This maximum, called the MUF, is given by

$$\omega_M = \omega_p \{\nu_M/\delta_M\}^{1/2}, \tag{32a}$$

$$\nu_M = \nu(\overline{h}_M), \delta_M = \delta(\overline{h}_M), \tag{32b}$$

$$\overline{h}_M \approx \overline{h}_{n+1} = h_o + \sigma \ln[(\overline{h}_n/2\sigma)\{1+(2\overline{h}_n/D)^2\} - 1], \tag{33}$$

$$\overline{h}_1 = h_o, \quad n = 1, 2, \ldots$$

This procedure works reasonably well as long as D is not too near zero and $h_o > 2\sigma\{1+\ln(D/4\sigma)\}$. At vertical incidence, ω_M approaches ω_p as $\overline{h}_\tau$ goes to infinity. At oblique incidence, signal components are reflected back to the receiver from two different heights, giving rise to the so-called low $(\overline{h}_\tau \leq \overline{h}_M)$ and high $(\overline{h}_\tau > \overline{h}_M)$ rays. Components at frequencies greater than ω_M usually pass on through the ionosphere, although returns caused by scattering processes are sometimes received at higher frequencies.

The amplitude of the pulse response in (27) involves the second frequency derivative of the phase of the channel transfer function,

17

$$\phi"(\omega) \ = \ d\phi'/d\omega \ = \ (d\overline{h}/d\omega)d\phi'/d\overline{h}$$

$$= \ (2\alpha/\omega_p)(\delta)^{1/2}/\nu a, \tag{34}$$

$$a \ = \ (1-1/\delta)-(2\sigma/\overline{h})(1-1/\nu), \tag{35}$$

with the quantities being evaluated at $\omega = \omega_T$. The derivation of (34) makes use of the relationships

$$d\nu/d\overline{h} \ = \ -2(\nu-1)/\overline{h}, \ \ d\delta/d\overline{h} \ = \ -(\delta-1)/\sigma, \tag{36a}$$

$$d\omega/d\overline{h} \ = \ (\omega_p/2\sigma)(\nu/\delta)^{1/2}a. \tag{36b}$$

With $|H(\omega)| \approx 1$, the amplitude of a single term of (27) becomes

$$amp \ \approx \ |(f_p/2\alpha)\nu_T a_T/(\delta_T)^{1/2}|^{1/2}|S_T(\omega_T)S_R(\omega_T)|, \tag{37}$$

where $a_T = a(\overline{h}_T)$.

The phase of that portion of the pulse response that arises only from the channel transfer function (i.e., the phase θ of the impulse response),

$$\theta(\omega_T) \ = \ -\phi(\omega_T)+\omega_T\phi'(\omega_T), \tag{38}$$

involves an approximation to ϕ in the case of oblique incidence (D>0). For the low and the high rays, ϕ is approximated by (19) and (21), respectively, with $\omega = \omega_T$. The derivative ϕ' is obtained from (15):

$$\phi'(\omega_T) \ = \ (2\overline{h}_T/c)(\nu_T)^{1/2}, \tag{39}$$

These equations enable the simulation model (deterministic base) pulse response to be computed for a given ionospheric layer configuration and propagation path distance. As the path distance goes to zero, the response reduces to the values expected for vertical incidence, and the high ray

disappears. In addition to the pulse response, (29)-(31) can be used to plot delay vs. frequency traces similar to the displays of ionograms.

The total response at the receiver is, of course, the sum of pulse responses from all reflections. These may be caused by multiple layers in the ionosphere or by multihops from one layer. Modifications to the single-mode amplitude given by (37) may be introduced to account for the effects of ground reflections or absorption by intervening layers, although no explicit factor has been used in the comparisons that follow.

The influence of an intervening layer on the trace of an ionogram can also be simulated in the present model, but this is not yet included in the current pulse response computer program. For instance, if an E layer is present, frequency components that pass through and then are reflected back from the F layer show a characteristic retardation near the E layer critical frequency f_{pE}. This can be accounted for in the model by adding an E layer term to (8):

$$\bar{h} = h_o - \sigma \ln\{(f_p/f)^2 - 1\} - \sigma_E \ln|(f_{pE}/f)^2 - 1|, \quad f_{pE} < f < f_p. \tag{40}$$

An indication of the merit of (40) is shown in Figure 3, which compares the equation with an actual data sample. The measured points (denoted by X) are taken from Figure 4(a) of CCIR (1980) and represent measurements from an ionogram recorded at Argentine Islands in the fall of 1958. The penetration frequencies, σ's, and h_o were found by a simple fitting procedure to the measured ionogram:

h_o (km)	σ (km)	f_p (MHz)	σ_E (km)	f_{pE} (MHz)
260	34.0	8.2	39.3	2.4

The model appears to provide a reasonable fit to the actual ionogram.

3.2 Scattering Function

For the IPM to simulate actual conditions, the parameters that characterize the ionosphere must be allowed to change with time. For instance, a slow variation of layer height will cause a corresponding variation in the delay time of the pulse response; an example of this is shown in the
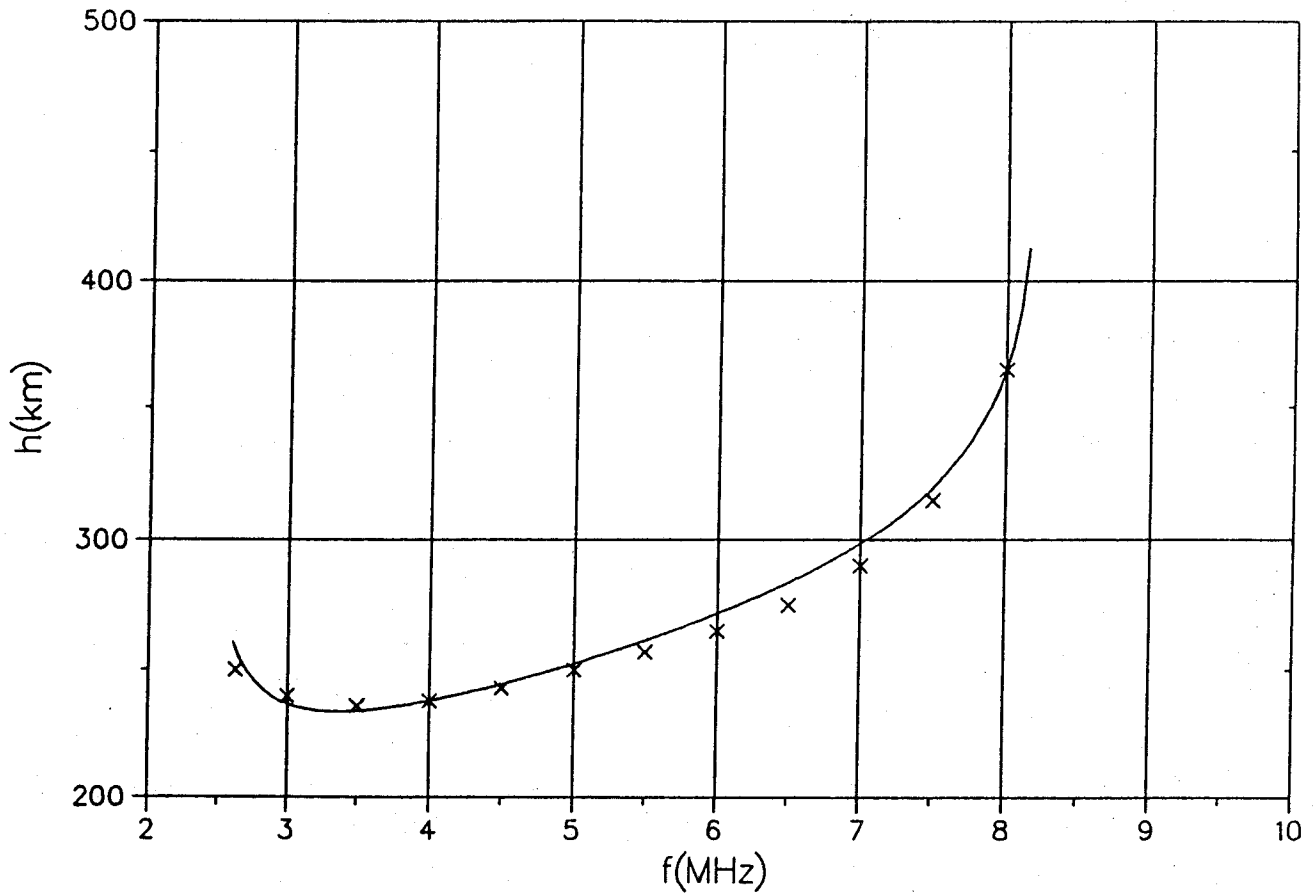
19

Figure 3.   Comparison of (3.19) with measured points (X's) from an ionogram
recorded at Argentine Islands in the fall of 1958.

comparisons of Section 4. Parameter changes (with time) will also lead to Doppler frequency shifts f_D that can change the phase characteristics of received signals.

A useful representation that describes received signal phenomena and complements the pulse response is the scattering functions $S(\tau, f_D)$ (Proakis, 1983; Ch. 7). This can be thought of as the power spectrum of contributions in the delay interval $\tau + \Delta\tau$ that cause a relative frequency shift in the range $f_D + \Delta f_D$. The scattering function is evaluated as the Fourier transform of the (complex) received signal autocorrelation function $R(\tau, \Delta t)$:

$$S(\tau, f_D) = \int_{-\infty}^{+\infty} R(\tau, \Delta t) \exp(-i2\pi f_D \Delta t) d(\Delta t), \qquad (41)$$

$$R(\tau, \Delta t) = E[z^*(\tau, t)z(\tau, t+\Delta t)], \qquad (42)$$

where $z(t)$ represents the complex signal and the asterisk denotes conjugation; $E[\cdot]$ is the usual symbol for expected value.

The Doppler frequency f_D is here defined as the time derivative of the phase of the received signal at a constant delay τ. Treating the phase as a function of t, we may rewrite (38) as

$$\theta(t) = \theta_\tau + (d\theta/dt)t \equiv \theta_\tau + 2\pi f_D t, \qquad (43)$$

Where θ_τ is a constant for given τ. The variation of $\omega_D = (d\theta/dt)$ over time depends on the time variation of ionospheric layer heights, thicknesses, and penetration frequencies. Investigation of this subject is one of the tasks proposed for future studies of the IPM.

For the simplest case of a constant Doppler shift, an indication of what one might expect the scattering function to look like for a wideband response is shown in Figure 4. The 0- and X-mode returns for a given F2 layer at vertical incidence have been used to obtain the plot, and the time variation is assumed to be such that the Doppler frequencies for the two returns are 0.167 and -0.02 Hz, respectively. The 0-mode delay spread $\approx 50\mu s$ and the X-mode spread is $\approx 24\mu s$; the power density (PD) plotted along the vertical axis has been normalized to a maximum value of unity. The scattering function shown
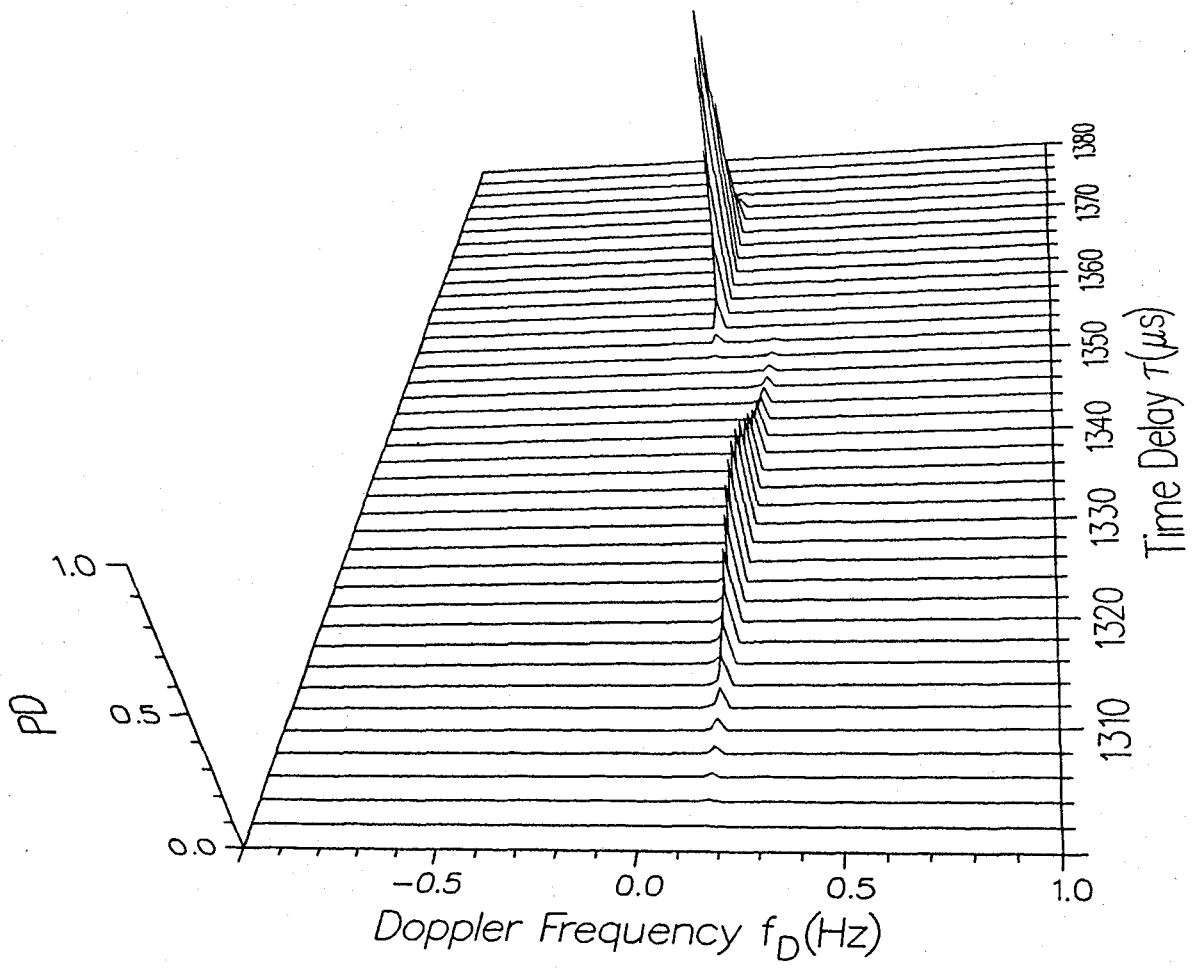
Figure 4. Example of constant Doppler frequency scattering function from the IPM.

here is similar to what one would obtain from the wideband NRL Channel Prober during stable conditions.

4.   COMPARISONS OF MEASUREMENTS WITH IPM

In the absence of independent measurements of the physical parameters describing ionospheric layers, IPM parameter values are obtained by fitting the tau-frequency relation (30) to measured ionogram traces. The penetration frequency is easily determined, and an estimate of the layer height and thickness follows by fitting (30) to the measured trace and solving for h_0 and σ.

Figure 5 reproduces an ionogram from the NRL Channel Prober taken over a 126-km path in southern California (Wagner and Goldstein, 1985). The instrument is acting as a narrowband (125 kHz) sounder with an amplitude threshold to eliminate most of the noise. A simulation of the one-hop F2 layer return is presented in Figure 5b showing the 0 and X modes and the crossover that occurs before the critical frequencies are reached. No knowledge of the actual layer conditions was available, so the simulation inputs were obtained by fitting the analytic functions to the measurement traces. For the ordinary mode, the results were f_p = 12 MHz, σ = 30 km, h_0 = 260 km; for the extraordinary mode f_p = 13 MHz, σ = 28 km, h_0 = 275 km. The model appears to provide a reasonable simulation of the return, at least as a reference base. Because of stable conditions during the measurement period (a fall morning), statistical effects are of minor importance.

Figure 6 reproduces the wideband (1 MHz) response at a center frequency of 5.5 MHz. A slow variation of layer height evidently occurred over a 10-minute interval of the measurement. Both the 0 and X modes show a slight variation of delay time, and this is achieved in the model by varying the height input h_0. The different delay widths of the two modes are obtained by fitting to the measured data. The cause of the null near the beginning of the ordinary mode response is unknown, and no attempt has been made to duplicate this in the simulation.

Figure 7 reproduces a portion of an ionogram taken by the NRL Channel Prober on a 2200-km path from Florida to New York. The low and high ray returns from a layer are shown for a junction frequency of $\approx$ 20 MHz, and both the 0 and X modes are present in the high ray. Actual layer conditions are
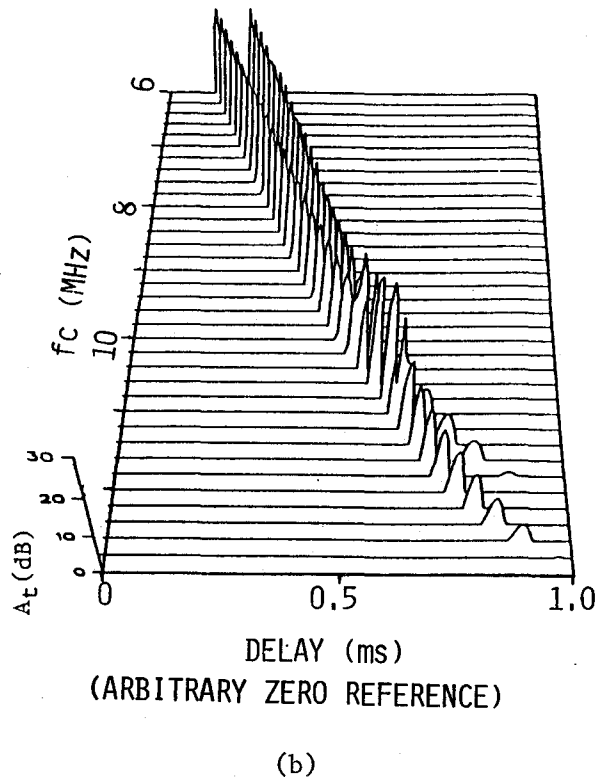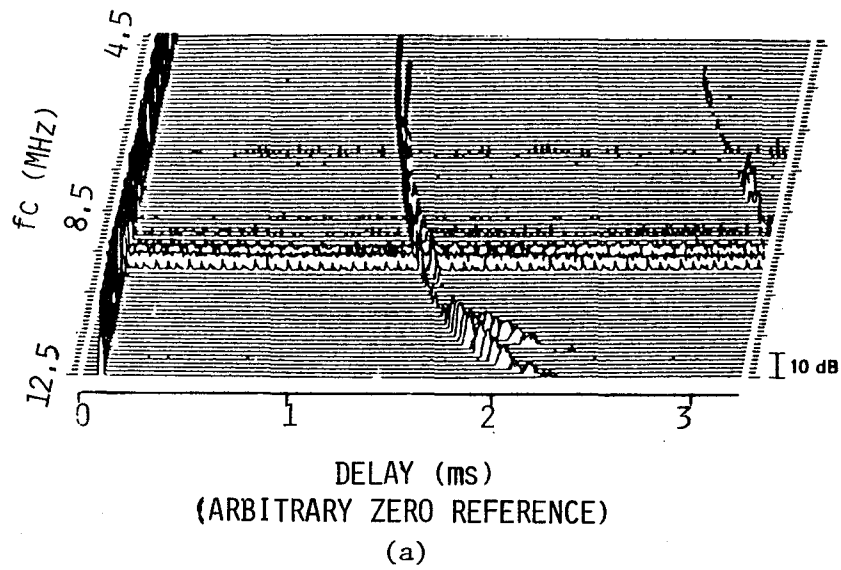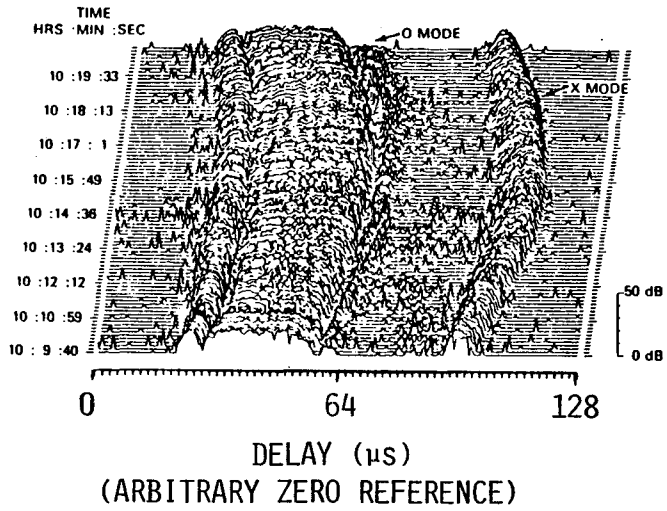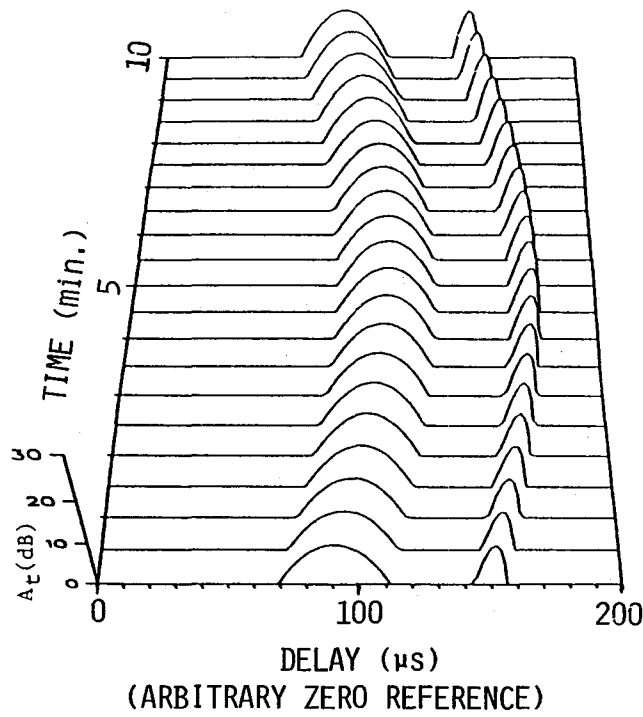
23

Figure 5. Measurement (a) and simulation (b) of a one-hop F_2 ionogram from the NRL Channel Prober. The path distance is 126 km, and the time is a fall morning.
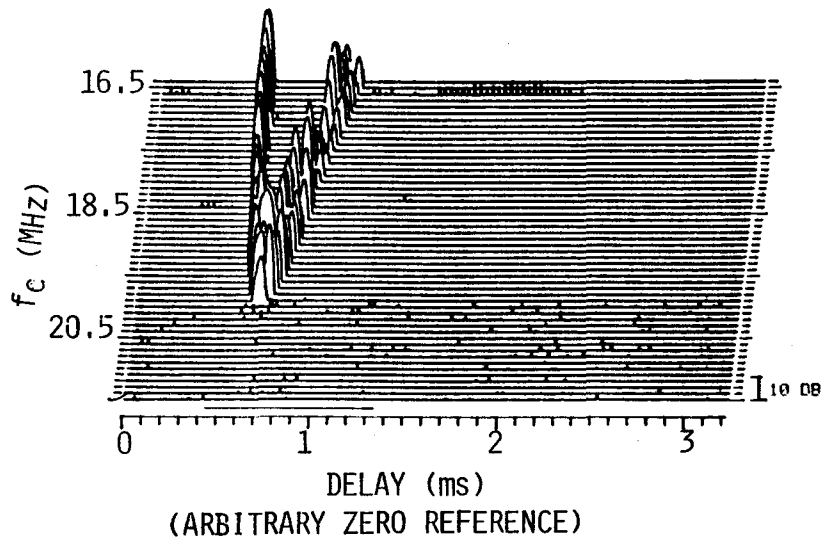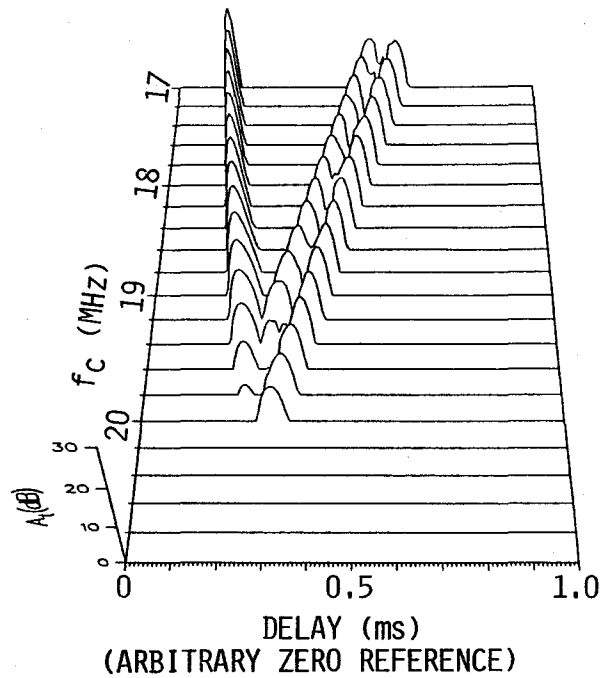
(a)

(b)

Figure 6.   Measurement (a) and simulation (b) of the time history of the F_2 mode of Figure 5 at 5.5 MHz.

25

Figure 7.   Measurement (a) and simulation (b) of an NRL Prober ionogram near
the junction frequency.   The channel is a 2200-km path from Florida
to New York.

unknown, but a fair representation of the response is obtained by assuming h_o = 294 km, σ = 30 km, and f_p $\approx$ 8 MHz. It should be pointed out that the origin of the delay scale for the measured ionogram has been offset by about 6 ms.

The applicability of the model to multiple returns is investigated in Figure 8, which shows a simulation of an ionogram taken over a 2600-km path from Colorado to New York. Three modes were assumed in the simulation with h_o values of 300, 400, and 520 km. Since there was no indication of what the layer thickness might be, σ = 30 km was used in all three modes. Junction frequencies were estimated from the measured ionogram, and from these were obtained approximate values for f_p: 7, 6.8, and 7.3 MHz. X modes were assumed in the high rays of both the first and third returns, so these inputs varied slightly from the 0 mode inputs. A simple random function was introduced into the pulse width parameters of the second return and the X mode of the third return, the purpose being only to see what effect this would have on the delay dispersion.

Simulation of Z-mode propagation, along with the 0- and X-modes, is shown in Figure 9. The measured ionogram is from Reber (1956), and the simulation (of the lower traces) is achieved by assuming three different values for the penetration frequencies and layer heights. The values used in the simulation of the lower trace are f_p(MHz) = 4.5, 5.3, 5.8, and h_o(km) = 284, 300, 308. The comparison displayed here emphasizes the importance of having a realistic frequency-delay time relationship in any model purporting to simulate wideband communication. Whether evaluating modems, protocols, or systems, a model restricted to stable configurations and slowly varying frequency ranges will not allow an adequate testing of performance under the wide variety of conditions encountered in actual practice.

The so-called "pulse prints" of the NRL Channel Prober can be simulated by the IPM if the phase term of the pulse response is modified to include the Prober signal detection process. The phase of the received signal is mixed with a local oscillator signal at the appropriate carrier frequency f_c and, after filtering and further processing, a translated and modified phase $\hat{\theta}$ is obtained. An analytic expression that simulates the pulse print pattern is

15.0

17.0

19.0

21.0

23.0

f_C (MHz)

0   1   2   3

DELAY (ms)
(ARBITRARY ZERO REFERENCE)

(a)

14

18

22

f_C (MHz)

30
20
10
0

A_t (dB)

0   0.4   0.6   0.8

DELAY (ms)
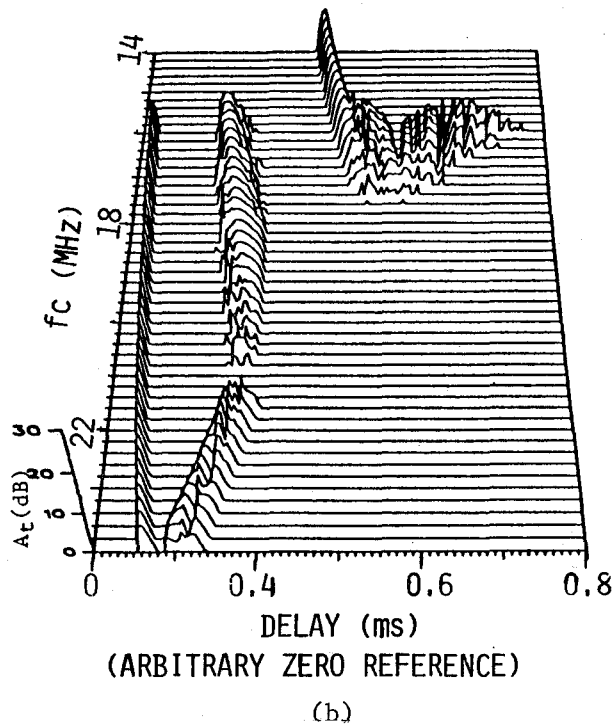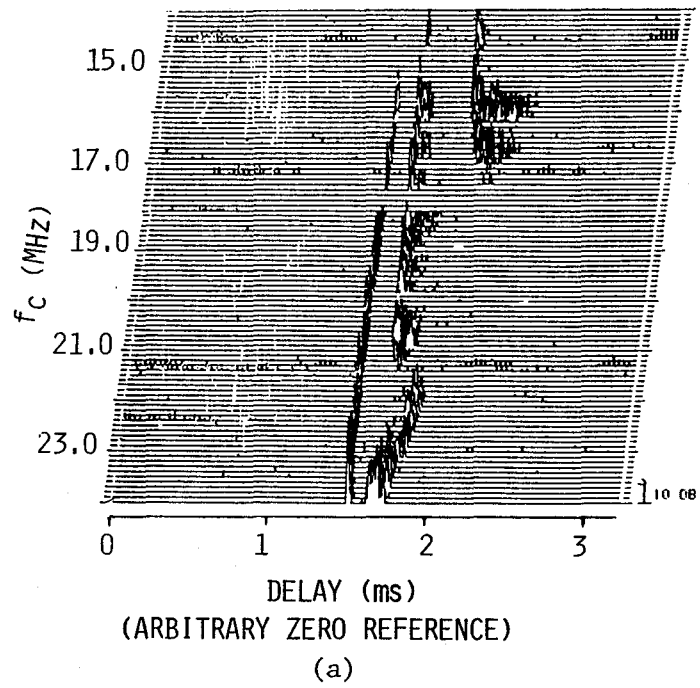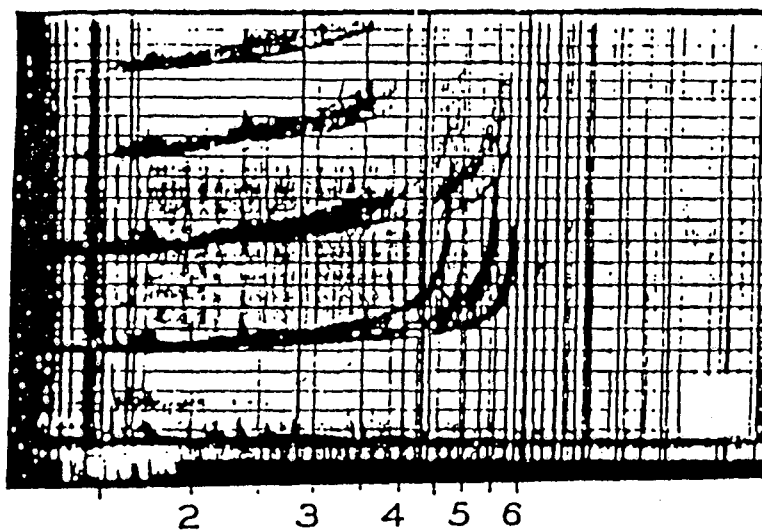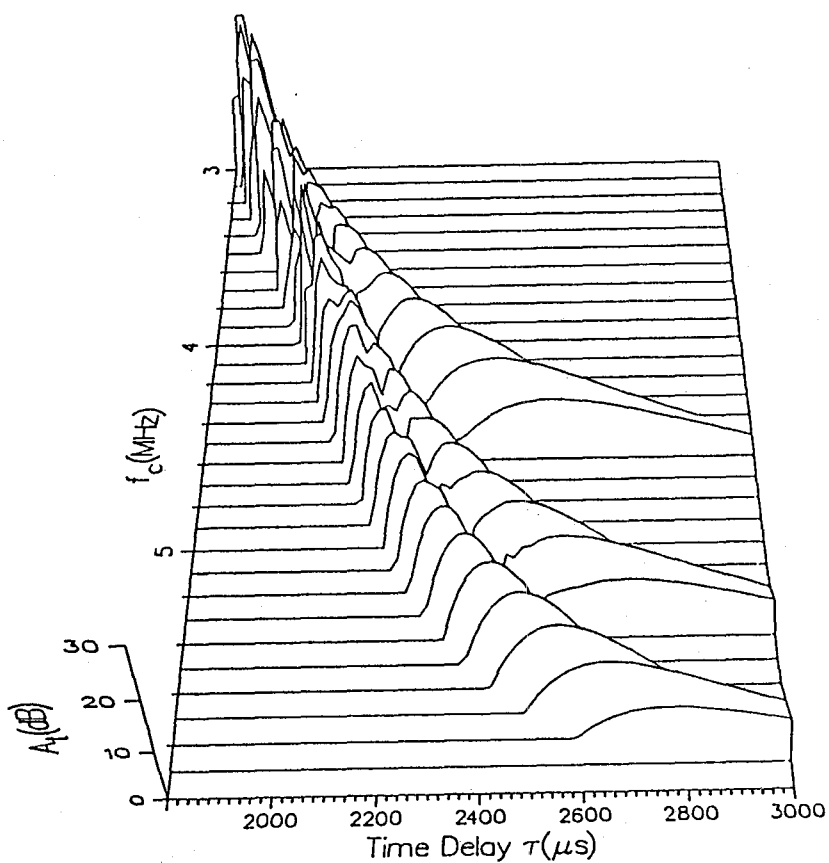(ARBITRARY ZERO REFERENCE)

(b)

Figure 8.   Measurement (a) and simulation (b) of an NRL Prober multi-mode
ionogram.   The channel is a 2600-km path from Colorado to New York.

28

(a)

(b)

Figure 9. Comparison of measured (a) and IPM model (b) ionograms showing Z-, O-, and X-traces.

$$\theta(f,t) = \hat{\theta}(f,t_o)+(d\theta/dt)t$$

$$= 2\pi\kappa(f-f_c)(\tau-\tau_c)+2\pi f_D t, \tag{44}$$

where τ_c is the delay time associated with f_c and κ is a constant dependent on the response width for a given mode. The Doppler frequency, $\omega_D = d\theta/dt$, is a function of the time variations of layer height and penetration frequency.

Figure 10 presents the simulation of a pulse print obtained by the NRL Prober over the same path as in Figure 5. Both the O- and X-modes are shown, but the simulation extends only over the first 30 seconds of time. The print represents the positive portion of the in-phase component of a signal received on a winter afternoon, and the mode Doppler frequency is constant over the time interval shown.

5. SUMMARY AND FUTURE WORK

This report describes the first phase of a two-phase project to develop a new HF channel simulation model. This model has general applicability for modeling a variety of channel propagation conditions and system bandwidths. The first phase of the project was to develop the deterministic portion of the model. The deterministic model must be capable of providing a "median" channel transfer function about which statistical variations can later be added. These statistical variations will be added during the second phase of the project.

The model must be capable of accurately representing the following conditions for sky-wave channels:

- arbitrary channel bandwidths from 1 kHz to several MHz
- channels featuring ordinary and extraordinary modes in both low- and high-ray returns
- channels that are very dispersive (e.g., spread-F and transauroral paths)
- channels that are nonstationary in either the time or frequency domains

Ideally, the model should be capable of modeling specific paths for specific propagation conditions. This requires specific statistical distributions for model parameters, not just ranges on those parameters.

The report describes the mathematical foundations for the deterministic portion of the Ionospheric Parameters Model. This is followed by comparisons

PROBER MODE, COHERENT I⁺, 1-HOP F2
DATE: 1/14/83
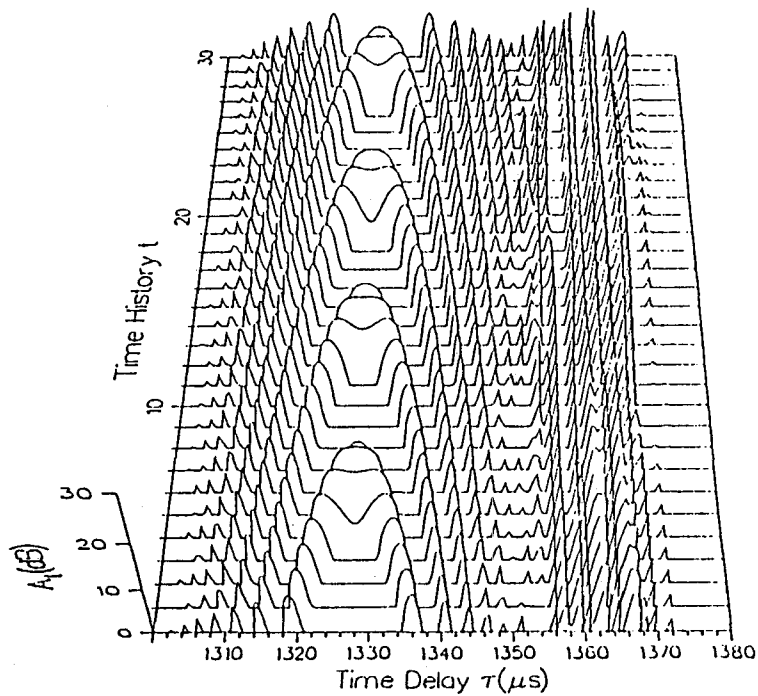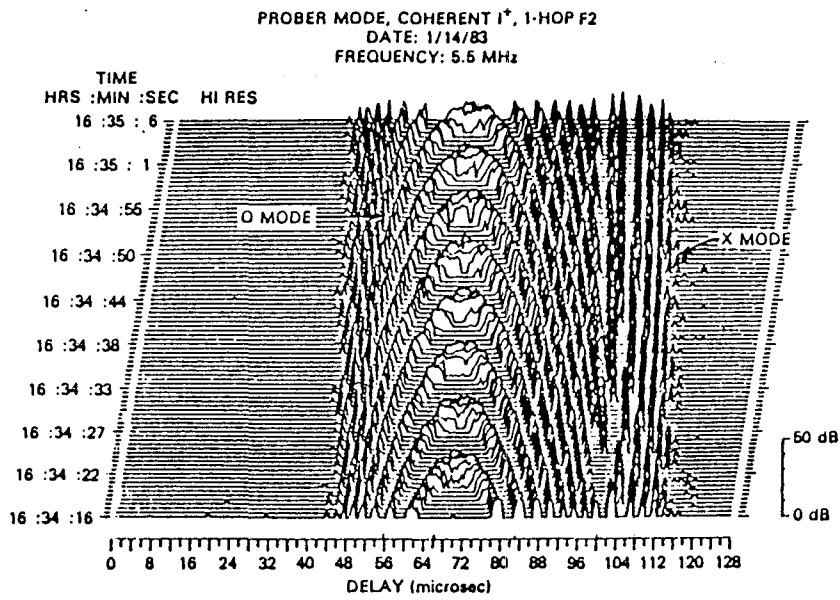FREQUENCY: 5.5 MHz

Figure 10.   Comparison of measured (a) and IPM model (b) pulse prints from same path as Figure 5.

between model output and empirical measurements made on several different paths. The paths include a vertical incidence path (Figure 3), a near vertical incidence path (126-km, Figures 5-6), and two long (greater than 2000 km, Figures 7-8) midlatitude paths. These comparisons demonstrate that the model is capable of producing wideband ionograms and time-history plots for channels having O- and X-mode magnetoionic components, and low- and high-ray paths. In this report, no comparisons between model output and measured data have been made for time dispersive channels. Such comparisons will be made in the near future. Results of the comparisons that have been made are encouraging. It is expected that this model, when complete, will be capable of meeting all of the objectives delineated above.

During the second phase of this project, the following work is planned:
- addition of the statistical time variations to the model
- additional comparisons of model output with computer plots of measured data (including ionogram, time-history, and scatter-function plots)
- quantitative verification of the model using empirical data
- creation of a functional block diagram for the eventual hardware implementation of the model in a hardware simulator
- identification of a methodology for predicting the median layer heights, layer thicknesses, and penetration frequencies as a function of geographical location, time-of-the-day, season, and sunspot number.

The latter is needed to meet the stated requirement that the model be capable of representing specific paths and specific propagation conditions, not just a range of conditions.

The model that will result from this work has applications for evaluation of both wideband communications and over-the-horizon radar systems. It can represent an extensive range of propagation conditions, and therefore is less restrictive than present narrowband HF channel models.

6. ACKNOWLEDGMENT

generosity in sharing data he collected using the Naval Research Laboratory wideband HF channel probe.

7. REFERENCES

Abramowitz, M., and I.A. Stegun (1964), Handbook of Mathematical Functions, Appl. Math. Ser., Vol. 55, (National Bureau of Standards, Washington, DC).

Baker, K.A., D.M. Haines, and B. Weijers (1986), Polar azimuth diversity HF propagation experiment, Rome Air Development Technical Center TR 86-11, Rome, NY.

Barratt, J.J., and T.L. Walton (1987), A real-time wideband propagation simulator for the high frequency band, Ionospheric Effects Symp., Naval Research Laboratory, Washington, DC, pp. 9-20.

Budden, K.G. (1961), Radio Waves in the Ionosphere, (Cambridge University Press, New York, NY).

CCIR (1974), HF ionospheric channel simulators, XIIIth Plenary Assembly, ITU, Geneva, Switzerland, Vol. III, Report 549, pp. 66-72.

CCIR (1980), Supplement to report 252-2 (Green Book), XIVth Plenary Assembly, Kyoto, Japan, 1978 (ITU, Geneva).

Dixon, R.C. (1984), Spread Spectrum Systems, (John Wiley and Sons, New York, NY).

Ehrman, L., L.B. Bates, J.F. Eschle, and J.M. Kates (1982), Real-time software simulation of the HF radio channel, IEEE Trans. Commun. COM-30, No. 8, pp. 1809-1817, Aug.

Girault, R., J. Thibault, and B. Durand (1988), Software ionospheric channel simulator, IEE Fourth Intl. Conf. on HF Radio Systems and Techniques, London, UK, IEE Pub. 284, pp. 321-325.

Haines, D.M. and B. Weijers (1985), Embedded HF channel probes/sounders, IEEE 1985 Military Commun. Conf., Boston, MA, Paper No. 12.1.

Hoffmeyer, J.A., and M. Nesenbergs (1987), Wideband HF modeling and simulation, NTIA Report 87-221, Jul., (NTIS** Order No. PB 88-116116/AS).

Hoffmeyer, J.A., and L.E. Vogler (1987), Measurement, modeling, and simulation of LOS microwave channels, NATO AGARD Conf. Proc., No. 419, Scattering and Propagation in Random Media, Rome, Italy, May, Paper No. 31.

**National Technical Information Service, 5285 Port Royal Rd., Springfield, VA 22161

Kelso, J.M. (1964), Radio Ray Propagation in the Ionosphere, (McGraw-Hill, New York, NY).

LeRoux, Y.M., G. Savidan, G. DuChaffaut, P. Gourvez, and J.P. Jolivet (1987), A combined evaluation and simulation system of the HF channel, IEE Fifth Intl. Conf. on Ant. and Prop., York, UK, IEE Pub. 274, pp. 171-175.

Malaga, A. (1985), A characterization and prediction of wideband HF sky-wave propagation, IEEE Military Commun. Conf., Boston, MA, Paper No. 12.5.

McRae, D.D., and F.A. Perkins (1988), Digital HF modem performance measurements using HF link simulators, IEE Fourth Intl. Conf. on HF Radio Systems and Techniques, London, UK, IEE Pub. 284, pp. 314-317.

Mooney, O.J. (1985), Implementation of an HF ionospheric channel simulator using a digital signal processor, IEE Third Intl. Conf. on HF Commun. Systems and Techniques, London, UK, pp. 27-31.

Papoulis, A. (1962), The Fourier Integral and its Applications, (McGraw-Hill, New York, NY).

Perry, B.D., and L.G. Abraham (1988), Wideband HF interference and noise model based on measured data, Report M88-7, MITRE Corp., Bedford, MA, Mar.

Perry, B.D., E.A. Palo, R.D. Haggarty, and E.L. Key (1987), Trade-off considerations in the use of wideband HF communications, IEEE Intl. Conf. Commun., Seattle, WA, Paper No. 26.2.

Proakis, J.G. (1983), Digital Communications, (McGraw-Hill, New York, NY).

Reber, G. (1956), World-wide spread F, J. Geophys. Res. $\underline{61}$, pp. 157-164.

Salous, S., and E.D. Shearman (1986), Wideband measurements of coherence over an HF skywave link and implication for spread-spectrum communication, Radio Sci. $\underline{21}$, No. 3, pp. 463-472, May-Jun.

Serrat-Fernandez, J., J.A. Delgado-Penin, E. Munday, and P.G. Farrell (1985), Measurement and verification of an HF channel model, IEE Third Intl. Conf. on HF Commun. Systems and Techniques, London, UK, IEE Pub. 245, pp. 52-56.

Skaug, R. (1982), An experiment with spread spectrum modulation on an HF channel, IEE Second Conf. on HF Commmun. Systems and Techniques, London, UK, IEE Pub. 206, pp. 76-80.

Skaug, R. (1984), Experiment with spread spectrum modulation on an HF channel, IEE Proc. $\underline{131}$, Part F, No. 1, Feb., pp. 87-91.

Vogler, L.E. (1984), Impulse response for ionospheric reflection with a sech^2 profile, Radio Sci. $\underline{19}$, No. 6, pp. 1543-1551.

Vogler, L.E. (1985), A note on pulse distortion by ionospheric reflection, IEEE Trans. Ant. Prop. $\underline{AP\text{-}33}$, No. 10, pp. 1151-1154.

Vogler, L.E., J.A. Hoffmeyer, J.J. Lemmon, and M. Nesenbergs (1988), Progress and remaining issues in the development of a wideband HF channel model and simulator, NATO AGARD Conf. Proc., Propagation Effects and Circuit Performance of Modern Military Radio Systems with Particular Emphasis on those Employing Bandspreading, Paris, France, Oct., Paper No. 6 (in press).

Wagner, L.S. (1987), Characteristics of mid-latitude sporadic E observed with a wideband HF channel probe, Radio Sci. 22, No. 5, pp. 728-744, Sept.-Oct.

Wagner, L.S., and J.A. Goldstein (1985), High-resolution probing of the HF ionospheric skywave channel: F_2 layer results, Radio Sci. 20, No. 3, pp. 287-302, May-Jun.

Wagner, L.S., J.A. Goldstein, and E.A. Chapman (1983), Wideband HF channel prober: system description, Tech. Report, Naval Research Laboratory, Washington, DC, Mar.

Wagner, L.S., J.A. Goldstein, and W.D. Meyers (1987a), Wideband probing of the trans-auroral HF channel, IEEE 1987 Military Commun. Conf., Washington, DC, Paper No. 43.2.

Wagner, L.S., J.A. Goldstein, and W.D. Meyers (1987b), Wideband probing of the trans-auroral HF channel: solar minimum, Ionospheric Effects Symp., Naval Research Laboratory, Washington, DC, pp. 31-43.

Watterson, C.C. (1981), HF channel-simulator measurements on the KY-870/P FSK burst-communication modem-set 1, NTIA Report CR-81-13, (NTIS[**] Order No. PB 82-118944).

Watterson, C.C. (1982), HF channel-simulator measurements on the KY-879/P FSK burst-communication modem-set 2, NTIA Contractor Report CR-82-20, Dec., (NTIS[**] Order No. PB 83-194738).

Watterson, C.C. and R.M. Coon (1969), Recommended specifications for ionospheric noise simulators, ESSA Tech. Report ERL-127-ITS-89.

Watterson, C.C., J.R. Juroshek, and W.D. Bensema (1969), Experimental verification of an ionospheric channel model, ESSA Tech. Report ERL-112-ITS-80.

Watterson, C.C., J.R. Juroshek, and W.D. Bensema (1970), Experimental confirmation of an HF channel model, IEEE Trans. Commun. Technol. COM-18, pp. 792-803.

Wetzel, L. (1967), On the theory of signal distortion due to ionospheric dispersion, Pap. Inst. Def. Anal., P-317, pp. 15-31.

APPENDIX

In Section 2.1, the transfer function of the IPM is obtained by applying asymptotic formulas to the gamma functions of the reflection coefficient (4). Another way of deriving the phase and its first derivative, given by (6) and (7), is the following.

For the case of no magnetic field and negligible electron collision frequency, the W.K.B. solutions to Maxwell's equations for the electric field E can be expressed as (see pp. 133-136 in the Budden reference of Section 7)

$$E(z) \approx A \exp\{\mp ik\int_o^z \mu dz\}, \tag{A1}$$

where A is a constant, $k = 2\pi f/c$ is the wave number, z is height above ground, and μ denotes the index of refraction of the ionosphere. Under the present assumptions, μ may be given the form

$$\mu = \{1-(f_N/f)^2\}^{1/2}, \tag{A2}$$

where f_N, the plasma frequency, is a function of height and ionospheric layer parameters.

The minus and plus signs in (A1) correspond to upgoing and downgoing waves, respectively, and if reflection occurs where $\mu = 0$ at the height z_o, then the reflection coefficient R is

$$R(\omega) = \exp\{-i2k\int_o^{Z_o}\mu dz\} = e^{-i\phi(\omega)}, \quad \omega = 2\pi f. \tag{A3}$$

If we assume the electron density profile of (3) and use (A2), then $\phi(\omega)$ and its derivative, $\phi' = d\phi/d\omega$, become

$$\phi = (2/c)\omega\int_o^{Z_o}[1-(f_p/f)^2 \mathrm{sech}^2\{(z_m-z)/2\sigma\}]^{1/2} dz. \tag{A4a}$$

$$\phi' = (2/c)\int_o^{Z_o}[1-(f_p/f)^2 \mathrm{sech}^2\{(z_m-z)/2\sigma\}]^{-1/2} dz. \tag{A4b}$$

The integrals in (A4a, b) are known respectively as the phase height h(f) and

equivalent (or virtual) height $\bar{h}(f)$ of reflection. Both integrals are expressible in closed form through the change of variable

$$\sinh\{(z_m - z)/2\sigma\} = C_o \cosh x, \quad C_o^2 = (f_p/f)^2 - 1, \tag{A5}$$

resulting in

$$\bar{h}(f) = 2\sigma x_1, \quad x_1 = \cosh^{-1}\{\sinh(z_m/2\sigma)/C_o\}, \tag{A6a}$$

$$h(f) = 2\sigma[x_1 - (f_p/f)\tanh^{-1}\{(f/f_p)\tanh x_1\}]. \tag{A6b}$$

If we impose the conditions $h_o = z_m \gg 2\sigma$ and $\bar{h}(f) \gg 2\sigma$, then the heights of (A6) approximate to

$$\bar{h}(f) \approx h_o - \sigma\ln\{(f_p/f)^2 - 1\}, \tag{A7a}$$

$$h(f) \approx \bar{h}(f) - \sigma(f_p/f)\ln\{(f_p + f)/(f_p - f)\}, \tag{A7b}$$

where use has been made of the relationships between inverse hyperbolic functions and the logarithm. The substitution of these expressions into (A4) yields the equations for ϕ and ϕ' given by (6) and (7).

BIBLIOGRAPHIC DATA SHEET

	1. PUBLICATION NO. NTIA Report 88-240	2. Gov't Accession No.	3. Recipient's Accession No.
4. TITLE AND SUBTITLE A New Approach to HF Channel Modeling and Simulation Part I: Deterministic Model			5. Publication Date **December 1988**
			6. Performing Organization Code NTIA/ITS
7. AUTHOR(S) L.E. Vogler & J.A. Hoffmeyer			9. Project/Task/Work Unit No.
8. PERFORMING ORGANIZATION NAME AND ADDRESS National Telecommunications and Information Admin. Institute for Telecommunication Sciences 325 Broadway Boulder, CO 80303			
			10. Contract/Grant No.
11. Sponsoring Organization Name and Address NTIA Herbert C. Hoover Bldg. 14th & Constitution Ave., NW Washington, DC 20230			12. Type of Report and Period Covered
			13.

14. SUPPLEMENTARY NOTES

15. ABSTRACT *(A 200-word or less factual summary of most significant information. If document includes a significant bibliography or literature survey, mention it here.)*

This report describes a new and unique approach for modeling either narrowband or wideband high frequency (HF) channels. Although narrowband models of the HF channel have existed for many years, they are applicable to only a limited set of actual propagation conditions. The need for an HF channel model that is valid for both narrow and wide bandwidths over a more extensive range of propagation conditions provided the motivation for the research documented in this report.

Continued on reverse

16. Key Words *(Alphabetical order, separated by semicolons)*

channel transfer function; HF channel models; HF propagation; over-the-horizon radar (OTHR); spread spectrum; wideband communications; wideband HF

17. AVAILABILITY STATEMENT ☒ UNLIMITED. ☐ FOR OFFICIAL DISTRIBUTION.	18. Security Class. *(This report)* unclassified	20. Number of pages 43
	19. Security Class. *(This page)* unclassified	21. Price:

15. ABSTRACT (continued)

The report describes the development of a channel transfer function for the HF channel that accurately models a wide variety of propagation conditions and can be used for the evaluation of wideband HF systems. The first part of this modeling effort has been to develop a model that represents the median channel conditions. Good agreement has been found between the model and wideband propagation measurements taken during relatively stable conditions. The report provides comparisons between ionograms generated by the model and measured wideband ionograms that have been reported in the literature. Encouraging results have also been found in comparing model outputs with measured time-history plots.